Scientific Student Associations' Conference 2023

Remote sensing based analysis of suspended sediment transport in rivers

by

Yousaf Muhammad Zaighum

and

Ameen Abdus Samad

Supervisors:

Dr. Sándor Baranya

Associate professor, Department of Hydraulic and Water Resources Engineering

Flóra Pomázi

Research fellow, Department of Hydraulic and Water Resources Engineering

Michael Nones

Associate Professor, Hydrology and Hydrodynamics Department, Institute of Geophysics Polish Academy of Sciences

Budapest, 2023

Abstract

The analysis of sediment transport in river systems is of immense importance for river researchers as the spatio-temporal variation of the sediments plays a crucial role in a wide spectrum of river uses, such as navigation, recreation, habitats or hydropower production. The advancement in technology has made it possible to use various indirect techniques to study and evaluate the transport of suspended sediment in fluvial environments. To investigate large-scale phenomena, remote sensing is becoming a largely utilized approach.

This research focuses on deriving suspended sediment concentration maps by combining satellite images with local monitoring data of suspended sediment concentration (SSC). For calibration purposes, the study analyzes two river sections: Danube River at Gönyű, Hungary, and the Raba River, a secondary tributary of the Danube. At these two sites we set up a model by relating in-situ SSC measurements with reflectance values extracted from satellite images. We tested various relationships for both rivers, to eventually derive a consistent relationship only for the Danube. Indeed, images of extracted from Raba were not considered reliable because of their coarse resolution with respect to the river dimensions, and the presence of clouds during relevant acquisition dates.

For the Danube though, the selected exponential model strongly correlates SSC and water reflectance and is here further used for mapping SSC in time and space along the Danube River, near the confluence with the Raba River. The established model can supply new insights into the spatial variation of sediment transport at hotspots of the river systems, such as confluence zones, barriers, reservoirs. Our study introduces examples for such applications.

Contents

1. Introduction

Sediments are key elements of river systems, as they determine the morphological changes of the river, influence the quality of habitats along the river, and it can affect different water uses such as drinking water supply, fluvial navigation, energy production, etc. Understanding the sediment transport processes is therefore important. In fact, quantitative information about the transported sediment is needed for the characterization of the river dynamics, as well as for providing information for engineering studies related to rivers, e.g., for planning of river restoration measures.

Considering the mode of the sediment transport, we distinguish the transport of coarse sediment particles at the riverbed, i.e., bedload, and the transport of fine sediments, mixed up in the water column, i.e., suspended sediment. The analysis of these two transport modes requires different approaches and methods. In this study, we focus on suspended sediment transport, which indeed plays an important role in e.g., floodplain, reservoir or side-arm sedimentation processes. The analysis of fine sediment transport can be very challenging at complex hydromorphological features, such as at river confluences.

In geography, a confluence occurs where two or more flowing bodies of water join to form a single channel. A confluence can occur in several configurations: at the point where a tributary joins a larger main river; where two streams meet to become the source of a river of a new name; where two separated channels of a river, forming a river island, rejoin at the downstream end. In all those cases, substantial variations of the hydrodynamics and ecological pattern and bed morphology occur. The point or region where the confluence occurs at that region the hydrodynamics are changed because of convergence and realignment of joining flows is called confluence hydrodynamic zone (CHZ). (Gualtier, 2018; Yuan et al., 2021).

For the investigation of the suspended sediment concentration (SSC) in rivers, lot of measurements and observation must be taken at the point of a confluence because of this reason it is impossible to get spatial view of the process in the whole region of confluence exclude the cross-section where the monitoring station is present. This is the reason why we should use satellite images instead of point samplings, to complete our sediment observations network (Curran & Novo, 2022). With respect to single-section measurements of SSC, satellite images can cover larger geographical areas with relatively high revisit time (i.e., temporal resolution), (Zhan et al., 2019). In literature, there are studies that have shown a

good mathematical correlation between measured SSC and spectral response properties of satellite images (Gholizadeh et al., 2016).

In the Yellow River Estuary, quantitative monitoring, and evaluation of suspended sediments were performed by using ETM+ images (ETM is Enhanced Thematic Mapper). In the same way, these measurements were taken in the Yangtze River (Luo et al., 2022), the Yellow River Estuary (Qiu et al., 2017), the Pearl River Estuary and macro-tidal Yalu River Estuary (Cheng et al., 2016). This above-mentioned research showed us that satellite Imaginary imagery is one of the effective ways to show SSC values in large confluence areas. Thus, if the satellite images are taken from one sensor it is not possible for large spatial scale or in the case of long-term studies, with the help of multi-source satellite images, which help in extracting of SSC value. This way is becoming famous nowadays– for research purposes. Such as: according to Gholizadeh et al. (2016) multispectral satellite is more possible for checking the quality of water in wide-scale waterbodies (e.g., coastal bodies and large lakes).

For the extraction approaches there are multiple ways, but nowadays empirical analysis of data based on linear regression and multi factor statistics are still in use. However, principal part analysis and artificial neutral network are effective alternative exact predictions. For small waterbodies it is still impossible to predict the low SSC values for remote sensing (Chelotti et al., 2019).

In this research we make an attempt to calibrate Sentinel-2A satellite images to assess suspended sediment transport processes in the Danube River and in its tributary, including a confluence zone. The main goal of this study is to work out an effective method to analyte satellite images for sediment transport assessment, to test different approaches for the quantification of SSC from the so-called reflectance values of the satellite images and to perform a calibration, based on which SSC maps can be generated for different hydrological situations. For calibration purposes, we use sediment data from two nearby sediment monitoring stations, one in the Danube mainstem at Gönyű, and one in the Raba River in Győr. At both sites, recently set up sediment monitoring stations provide continuous SSC data.

2. Materials and Method

2.1 Study Area

The study area (Figure 1) of the research is the Upper-Hungarian section of the Danube River, where the Raba River, a sediment-rich secondary tributary of the Danube flows into the mainstem through the Mosoni-Duna. The Danube is the second largest river of Europe and the most international river in the world. Its origin is in the Black Forest, in Germany and flows into the Black Sea, in Romania after 2850 river km (rkm). More than 2000 rkm of its length is navigable and also serves as a significant provider of both hydropower and drinking water. The Hungarian section belongs to the middle section, where the riverbed expands, and the bed slope significantly decreases - from approximately 40 cm/km to 10 cm/km. The mean annual flow discharge is around 2000 m^3/s, while the 100-year flood reaches 10,000 m^3/s. Within Hungary, the average water depth measures approximately 5 meters, and the river's typical width spans 350 meters. The mean total cross-sectional suspended sediment load is 40 kg/s (i.e., approximately 1.3 Mt/year), while the mean SSC is around 30 mg/l (Pomázi and Baranya, 2020).

Figure 1: Overview map of the study area and the location of the suspended sediment monitoring stations (blue: in the Danube; yellow: in the Raba) (source of map: Sentinel-2, 15.08.2023.)

In this research, one of the selected study sites is located at the 1790.60 rkm of the Danube near the settlement of Gönyű, just few rkms downstream of the confluence of the Mosoni-Duna and the Danube (1794 rkm). The other study site is in the Raba River, near Győr. The source of the Raba is the Austrian Alps, meaning that the suspended sediment of the tributary is also different than the Danube's. In fact, the SSC can reach a magnitude higher values than the SSC in the Danube, whereas its mean flow discharge is around 30 m^3/s only. The Raba River is not only characterized by a high suspended sediment content, but also carries a high amount of organic content that is washed in from the urban areas of Győr. The turbid water of the Raba is clearly distinguishable on satellite images (Figure 1), which makes this case study quite illustrative. At both sites, a continuously measuring suspended sediment monitoring station had been installed in 2022.

2.2 In-situ Measurements

The suspended sediment monitoring stations are equipped by calibrated Hach-Lange OBS (optical backscatter sensor; Figure 2) instruments, that continuously measure the SSC in a near-bank point of the monitoring cross sections. The sampling frequency is 1 minute, which qualifies as a very high temporal resolution. The continuous monitoring started in the end of April 2022. The SSC values measured in the rivers corresponding to the time when the satellite images were taken were extracted from time series recorded since on each stations. Furthermore, the daily distribution of the SSC data was also examined to filter the rapidly changing, non-permanent scenarios as they would introduce an additional source of uncertainties.

Figure 2: The Solitax sensor by Hach (source: hach.com)

2.3 Satellite Data and Image Processing

2.3.1 Satellite Data

In this study, the satellite images of the Sentinel-2 was used. The Copernicus Sentinel-2 mission consists of two polar-orbiting satellites positioned in a synchronized sun-synchronous orbit, with a 180° phase difference between them. The objective of this mission is to observe changes in land surface conditions. With its broad swath width of 290 kilometers and frequent revisits (10 days at the equator with one satellite, and 5 days with two satellites in cloud-free conditions, resulting in 2-3 days at mid-latitudes), it facilitates the monitoring of alterations on the Earth's surface. The images are available for every fifth day. For this study, the images were extracted and processed using the QGIS (Quantum Geographic Information System) software, as the API (application programming interface) data of the satellite is integrated into the GIS software.

The images used belong to Level L1C and Level L2A both. L2A images are the ones with atmospheric correction. However, L1C images are georeferenced but without atmospheric correction. (Table 1) The reference system used is EPSG:3857.

Table 1: Sentinel-2 product types (source: https://sentinels.copernicus.eu/)

Type	Code	Description	Users	Production&Distribution
User Product	Level-1B	Top-Of-Atmosphere radiances in sensor geometry	Expert Users	Systematic generation and online distribution
	Level-1C	Top-of-atmosphere reflectances in cartographic geometry	All Users	Systematic generation and online distribution
	Level-2A	Atmospherically corrected Surface Reflectances in cartographic geometry		

The images were examined between 02/05/2022 (i.e., the start date of the continuous measurement of SSC at the monitoring stations) and 31/07/2023. In the preparation stage, cloud-free images were chosen for the extraction of reflectance values. To increase the accuracy of the results, such images were also included which had minimal cloud cover but clear pixels over the study area. Then, the SSC availability for the date of the pre-selected images were verified. A compilation of different scenarios is shown in Figure 3. Figures 3a-c

illustrates examples of different flow conditions of the two rivers when: a) there is no significant inflow from the sediment-rich tributary, b) the sediment plume of the tributary enters the Danube under medium flow conditions (i.e., significant tributary influence), and c) there is high SSC in both rivers. Examples of different cloud cover are shown in Figures 3d-f. In total, 35 days were selected for the Danube section and 16 for the Raba site. The selected dates are found in the Appendix.

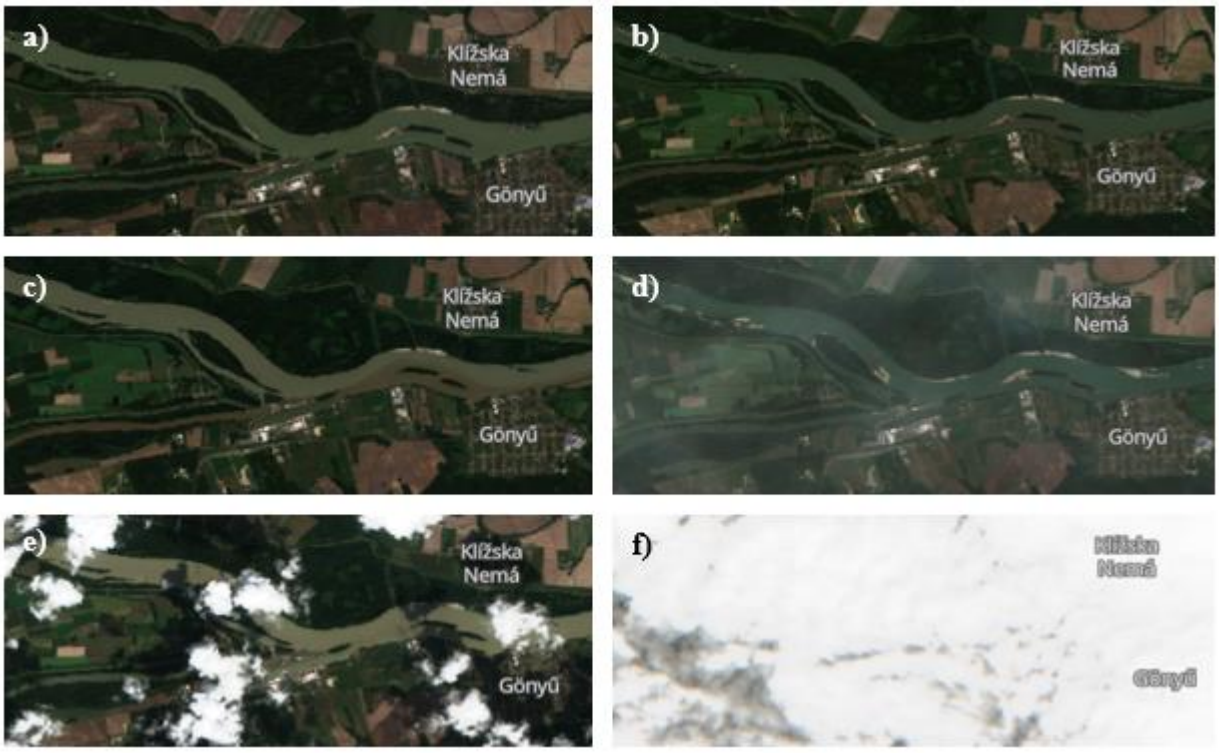

Figure 3: Examples of Sentinel-2 satellite images under different circumstances: a) no influence from the sediment-rich tributary, b) significant sediment-rich tributary influence, c) high SSC in both rivers, d) foggy weather, e) little cloud cover, and f) high cloud cover.

2.3.2 Image Processing

In QGIS, images are processed using the Semi-automatic Classification Plugin (SCP). The Semi-Automatic Classification Plugin, available as a free add-on for the open-source QGIS software, facilitates the semi-automatic supervised classification of remote sensing images. This tool streamlines the process of generating Regions of Interest (ROIs) for training by utilizing techniques such as region growing or the creation of multiple ROIs. It automatically computes and presents the spectral signatures of these training areas in a spectral signature plot. Furthermore, users have the option to import spectral signatures from external references or sources (Congedo, 2016).

Images are influenced by the atmosphere through processes like light scattering, light absorption, and light refraction. Among these, light scattering is typically the most prominent factor. (Chavez, 1988). The SCP Plugin includes a method called Dark Object Subtraction (DOS1) to effectively remove the impact of light scattering from the images. This correction method entails subtracting a constant Digital Number (DN) value from the entire digital image. A distinct constant is employed for each spectral band, with a unique set of constants applied from one image to another. (Chavez, 1988).

Overall, image processing includes selecting the images with minimal clouds, cloud cover is given in percentage in Download Products tab in SCP. One can quickly select the image by looking at the one with minimum cloud cover. Furthermore, under Sentinel-2 tab light scattering is eliminated by applying DOS1 correction (Congedo, 2016). When images are in radiance, they represent the raw measurements of light received by a satellite sensor. To make these images more useful for comparing different scenes and reducing variability, they are converted to TOA (Top of Atmosphere) reflectance. This accounts for both the reflectance of the Earth's surface and the influence of the atmosphere on the received light. This conversion normalizes the data for variations in solar irradiance (the amount of sunlight), making it easier to compare and analyze the information captured by the satellite across different conditions and times (Congedo, 2016). The two satellites Sentinel-2A and Sentinel-2B are equipped with Multi-Spectral Instrument (MSI). This instrument captures data across various spectral bands (Table 2), including four bands at 10 meters resolution in the visible spectrum, covering the wavelengths of blue (490 nm), green (560 nm), red (665 nm), and near-infrared (842 nm). Furthermore, there are six bands at 20 meters resolution, four of which are narrow bands in the vegetation red edge spectral range (705, 740, 775, and 865 nm), along with two longer bands in the shortwave infrared (SWIR) region (1610 and 2190 nm). Additionally, there are three bands at 60 meters resolution dedicated to tasks like atmospheric correction (443 nm for aerosols and 940 nm for water vapor) and cirrus cloud detection (1380 nm) (Segarra, 2020).

Table 2: Sentinel-2 band characteristics

Band Number	Band Description	Central Wavelength (nm)	Bandwidth (nm)
Band 1	Deep blue	443	20
Band 2	Blue	490	65
Band 3	Green	560	35
Band 4	Red	665	30
Band 5	Red-edge	705	15
Band 6	Red-edge	740	15
Band 7	Red-edge	783	20
Band 8	Near Infrared	842	115
Band 8A	Near Infrared narrow	865	20
Band 9	Water vapor	945	20
Band 10	Cirrus	1375	30
Band 11	Shortwave infrared 1	1610	90
Band 12	Shortwave infrared 2	2190	180

2.3.3 Calibration of reflectance

The output values of the image processing (i.e., the reflectance values) can be further utilized by raster calculations to derive the desired results such as SSC maps. Before that, a suitable model has to be developed for the calibration of spectral reflectance values. Many models can be found in the international literature – the selected ones are listed in Table 3.

Table 3: Selected models of calibration

Model	Reference
R705-R740	Härmä et al., 2001
R783/R490	Yuan et al., 2019
R665	Caballero et al., 2018
(R560+R705)/(R560+R665)	Hou et al., 2017
R665/R560	Hou et al., 2017
R705	Kallio et al., 2001
R490/(R443+R560)	Lathrop & Lillesand,1989
R783	Zhan et al., 2019
(R560-490)/(R560+490)	Erena et al., 2019
R783*R705/R490	Zhan et al., 2019
R705*R705/R490	Zhan et al., 2019
(R783/R490) + (R665/R560)	Zhan et al., 2019

In this study, these twelve models' suitability for calibration was tested. By setting up regressions between the different models and the near-bank measured SSC values, a comparison could be done to optimize the calibration for the Danube and the Raba.

2.3.4 Overview of the applied methodology

In summary, the steps of the analysis performed within this study are the followings: 1) a dataset of Sentinel-2 satellite images and corresponding SSC data from in-situ sensors were established based on the review of all Sentinel-2 images between May 2022 and August 2023; 2) the images were processed in QGIS to perform atmospheric correction and obtain the reflectance values for each bands; 3) different models were set up based on the band calculations; 4) which were correlated with the in-situ SSC values; 5) to choose the optimal model for calibration. With such a calibration at hand, a wide range of possibilities become available in SSC mapping. An overview of the applied methodology can be seen in Figure 4.

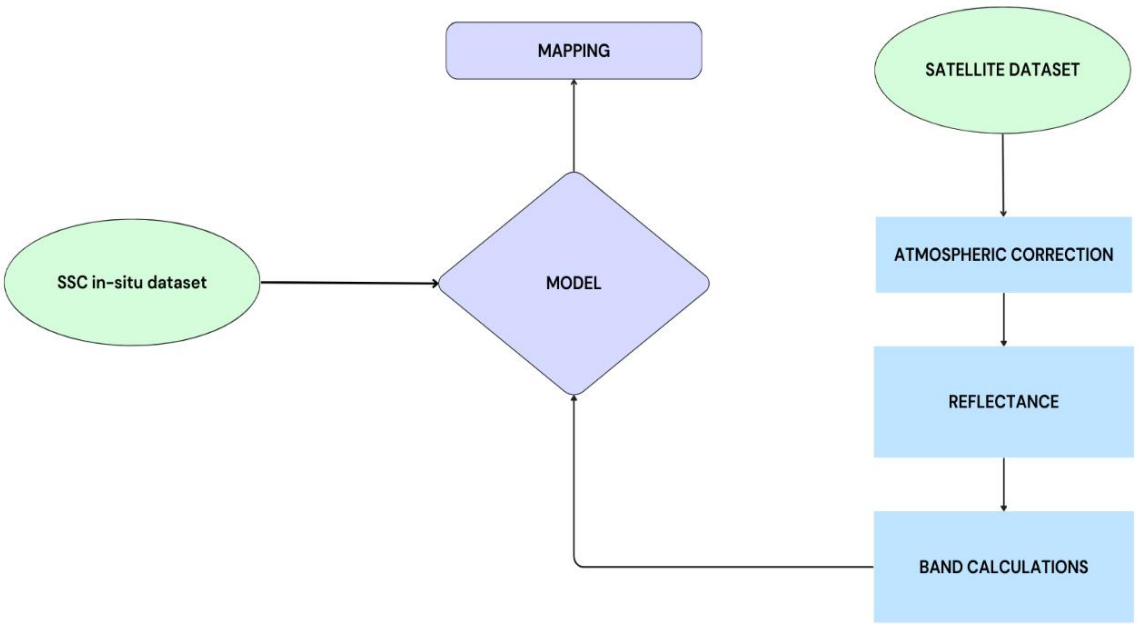

Figure 4: Overview of the applied methodology

3. Calibration

In most of the cases, the regression between the detected SSC and the applied model did not prove to be satisfactory (Figure 5). In each case, the type of regression was selected that resulted the best fit (i.e, the highest coefficient of determination, R^2). However, the data proved to be rather scattered. In fact, a set of outliers is apparent in many of the plots. As i) the measured data seems to be valid (i.e., no disturbances were detected in the measurement dataset), ii) this set is not always identified as outliers – in fact, iii) without these the R^2 would decrease, they were not excluded from the dataset.

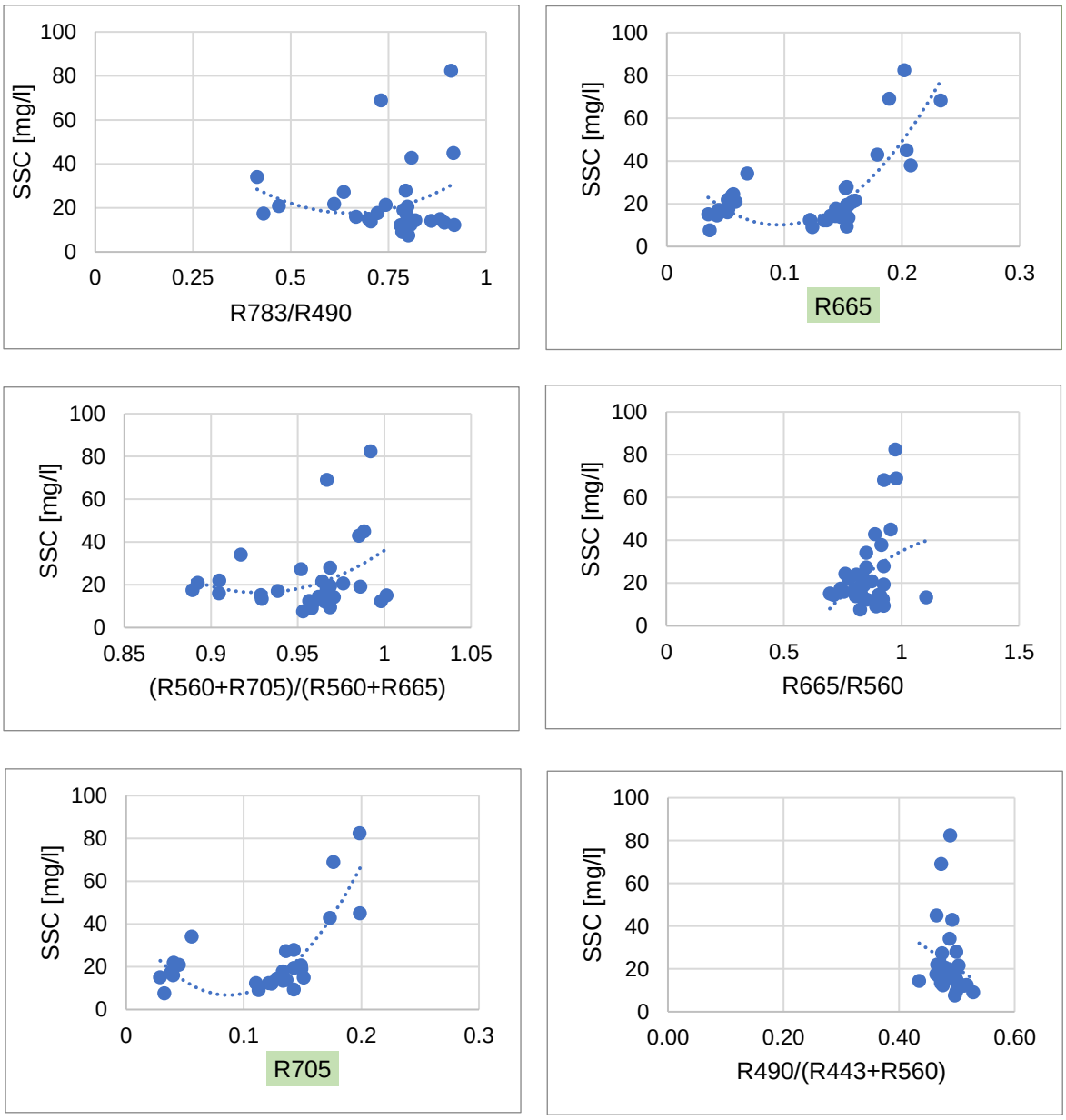

Figure 5a: Models for the Danube (the models with the good performances are highlighted in green) (part 1)

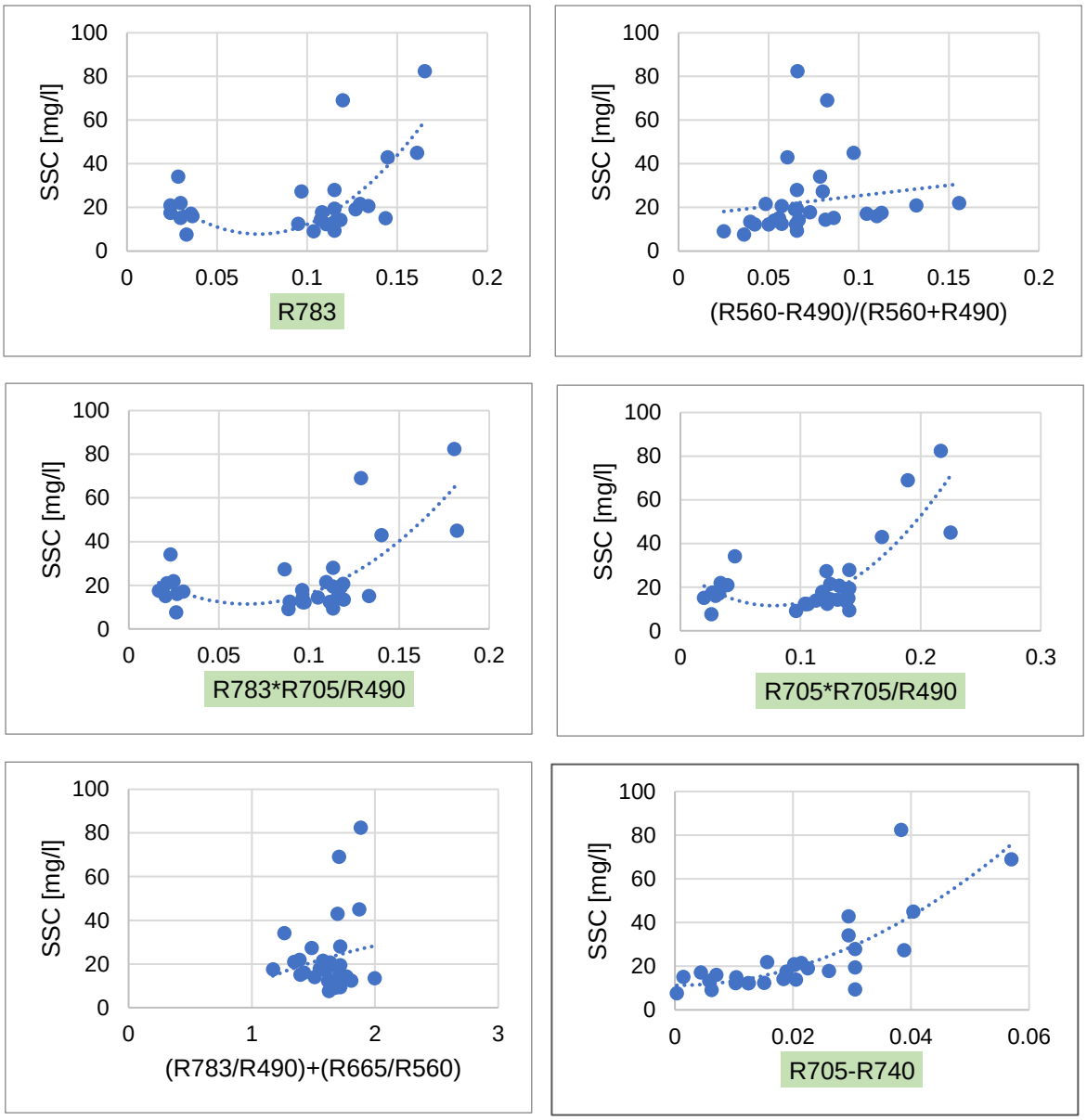

Figure 5b: Models for the Danube (the models with good performances are highlighted in green) (part 2)

The R705, R705*R705/R490, R665 and R705-R740 models proved to be the best fitted models - all of them has a coefficient of determination higher than 0.60. However, when comparing them visually, only the R705-R740 model has a continuous data on the detected range, so it was chosen as the best model (Figure 6). In this case, after filtering and analyzing the accuracy of data, 30 sample values was selected for calibration. This model performs well if the SSC is relatively low (i.e., < 20 mg/l). It is easy to obtain as its parameters are simple. and easily extracted. It must be noted that only a limited number of dates could be used when the Danube was characterized by a SSC higher than 30 mg/l. As a result of this, the established relationship is somewhat weaker in this range of SSC. It should be also

investigated in future research, whether the sediment-rich tributary confluence affect the near-bank SSC. In case of tributary influence, the correlated SSC may need some correction in order to take into account this effect when setting up the model.

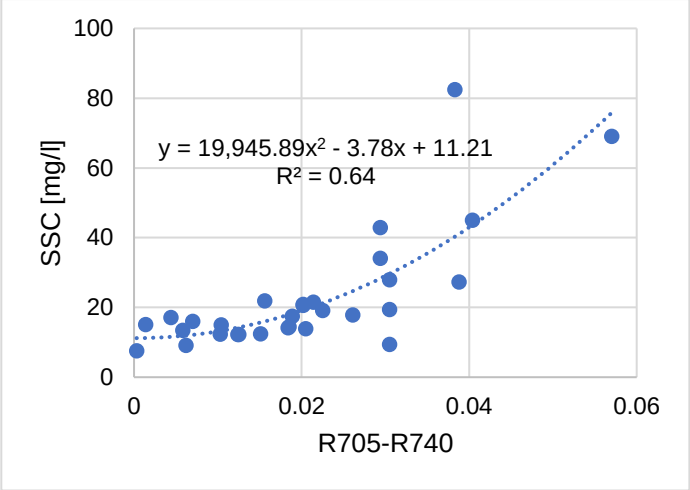

Figure 6: The final calibration curve for the Danube

Table 4 summarizes the main results of the applied models in the case of the Danube.

Table 4: Model results for the Danube (the models with the highest performances are higlighted in green)

Model	Type of best fit	R^2
R705	polynomial	0.69
R705*R705/R490	polynomial	0.67
R665	polynomial	0.65
R705-R740	polynomial	0.64
R783*R705/R490	polynomial	0.54
R783	polynomial	0.45
R665/R560	polynomial	0.15
(R560+R705)/(R560+R665)	polynomial	0.10
(R783/R490) + (R665/R560)	polynomial	0.08
R783/R490	polynomial	0.06
(R560-R490)/(R560+R490)	logarithmic	0.06
R490/(R443+R560)	linear	0.04

In the case of the Raba (Figure 7), the models' ranking is almost the same, though the performances are lower (the best fits are characterized by R^2=0.30-0.50). This is due to the fact that the SSC data of the Raba is rather scattered in itself as the dynamic processes of the suspended sediment transport in the sediment-rich tributary is a bit harder to capture reliably.

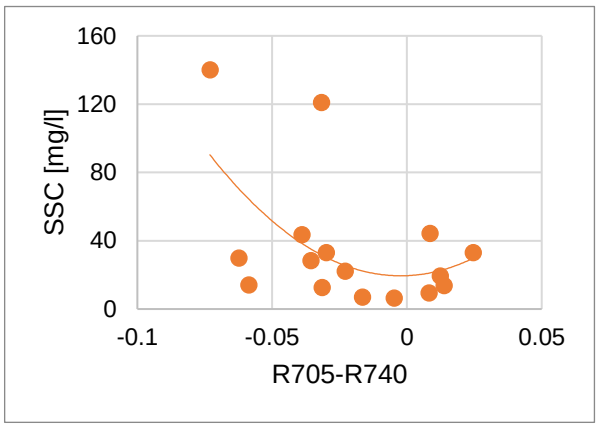
SSC [mg/l]
160
120
80
40
0
-0.1
-0.05
0
0.05
R705-R740

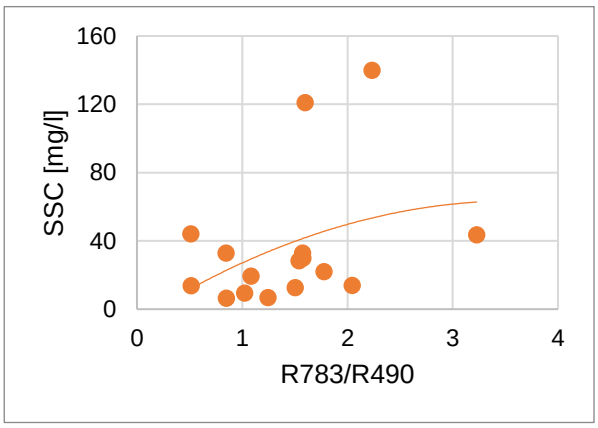
SSC [mg/l]
160
120
80
40
0
0
1
2
3
4
R783/R490

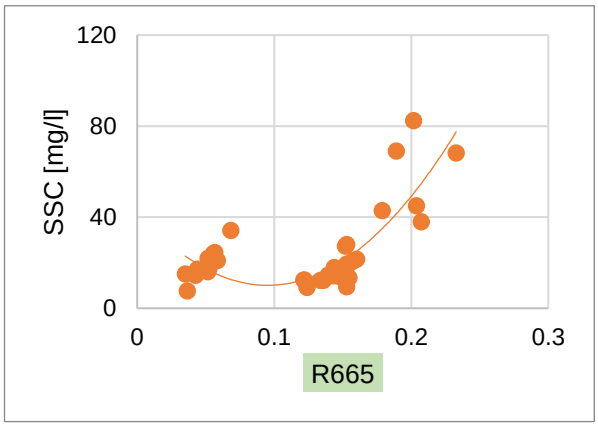
SSC [mg/l]
120
80
40
0
0
0.1
0.2
0.3
R665

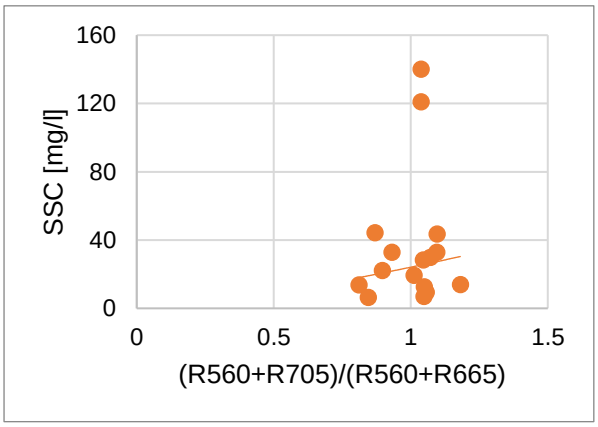
SSC [mg/l]
160
120
80
40
0
0
0.5
1
1.5
(R560+R705)/(R560+R665)

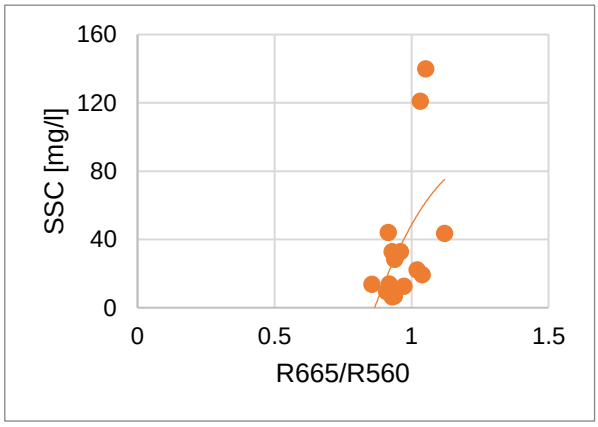
SSC [mg/l]
160
120
80
40
0
0
0.5
1
1.5
R665/R560

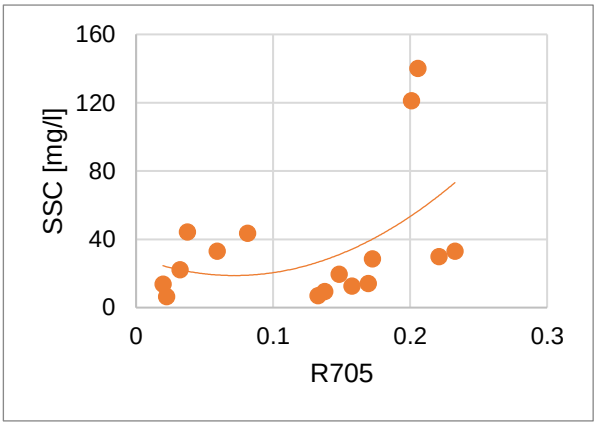
SSC [mg/l]
160
120
80
40
0
0
0.1
0.2
0.3
R705

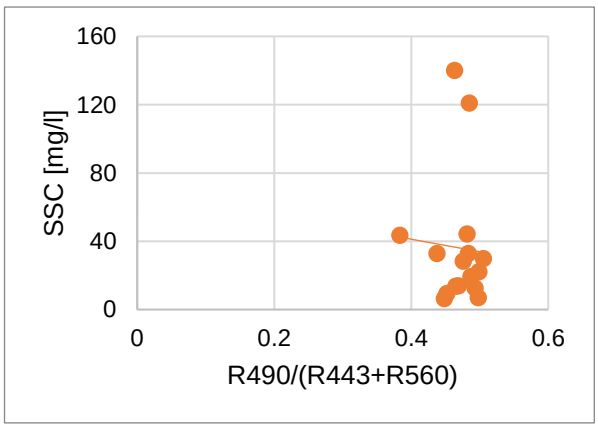
SSC [mg/l]
160
120
80
40
0
0
0.2
0.4
0.6
R490/(R443+R560)

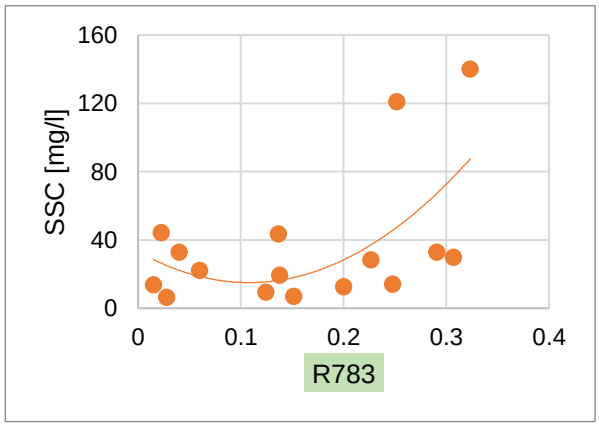
SSC [mg/l]
160
120
80
40
0
0
0.1
0.2
0.3
0.4
R783

Figure 2a: Models for the Raba (the models with good performances are highlighted in green) (part1)

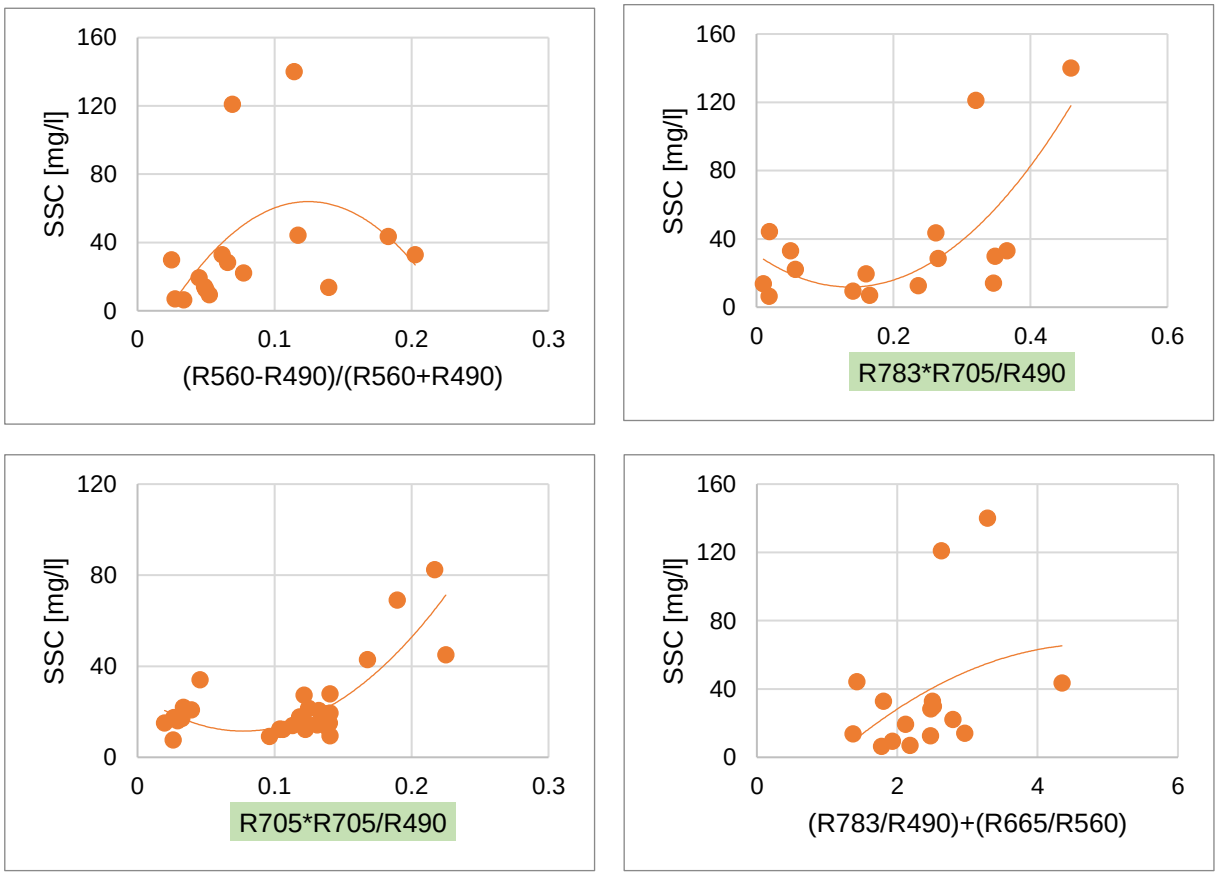

Figure 3b: Models for the Raba (the models with good performances are highlighted in green) (part2)

Table 5 summarizes the main results of the applied models in the case of the Danube.

Table 5: Model results for the Raba (the models with the highest performances are higlighted in green)

Model	Type of best fit	R^2
R783*R705/R490	polynomial	0.50
R705*R705/R490	polynomial	0.38
R665	polynomial	0.36
R783	polynomial	0.35
R705-R740	polynomial	0.28
R665/R560	polynomial	0.28
(R560-R490)/(R560+R490)	polynomial	0.24
R705	polynomial	0.20
(R783/R490) + (R665/R560)	polynomial	0.15
R783/R490	polynomial	0.13
(R560+R705)/(R560+R665)	linear	0.02
R490/(R443+R560)	linear	0.003

The corresponding models for the two rivers were further compared to each other to investigate whether a general model could be set up. It was found that more or less the same models work the best in each river's case (Table 6). The R490/(R443+R560) showed zero correlation in both cases. However, the lower goodness of the fits and the high scatter in the case of the Raba do not allow direct combination of models as of now – evidenced by visual evaluation of the datasets (Figure 8). In either case, the performance of the best models should be further improved before using them for different analyses of suspended sediment transport. Nevertheless, a discussion of the potential of the acquisition of SSC by using the remote approach presented and applied in this study is introduced in the next part of the study.

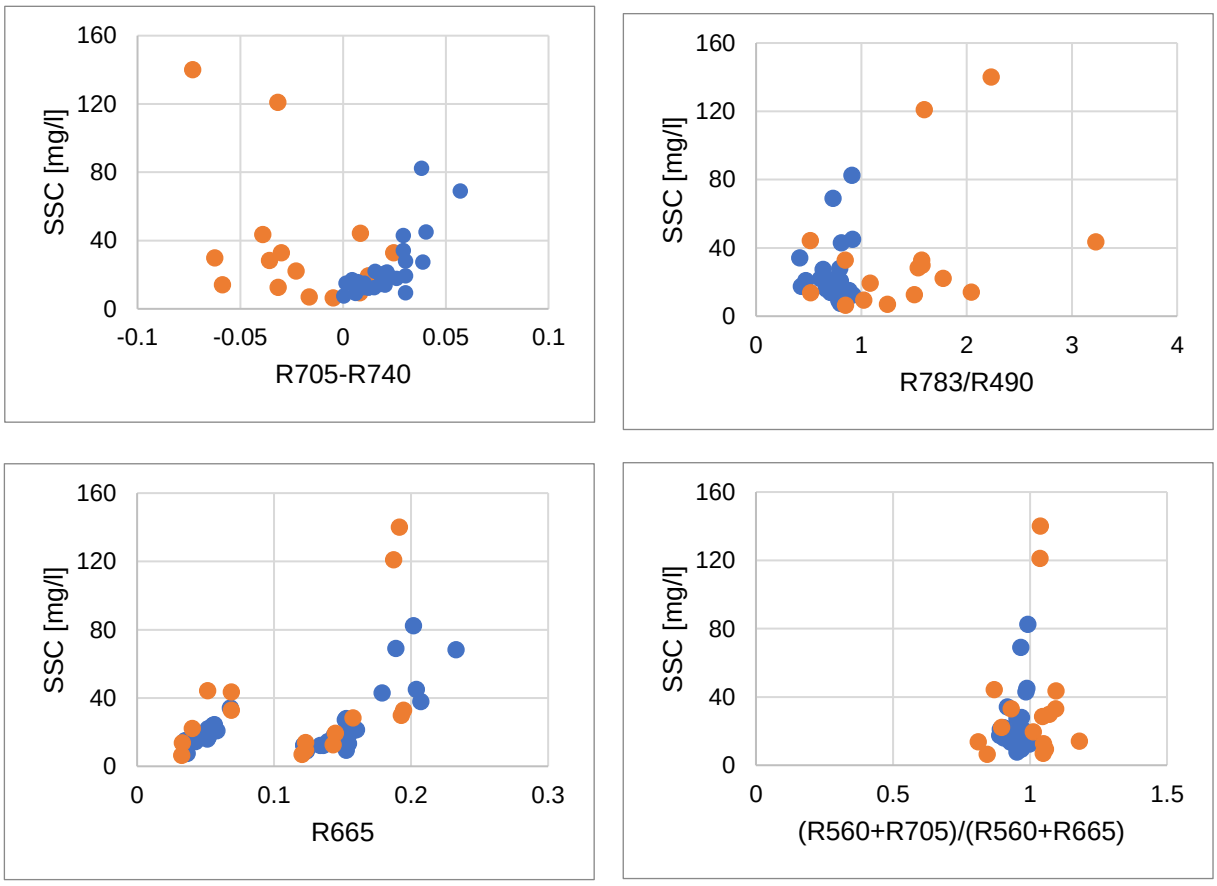

Figure 8a: Comparison of models (blue: Danube, orange: Raba) (part1)

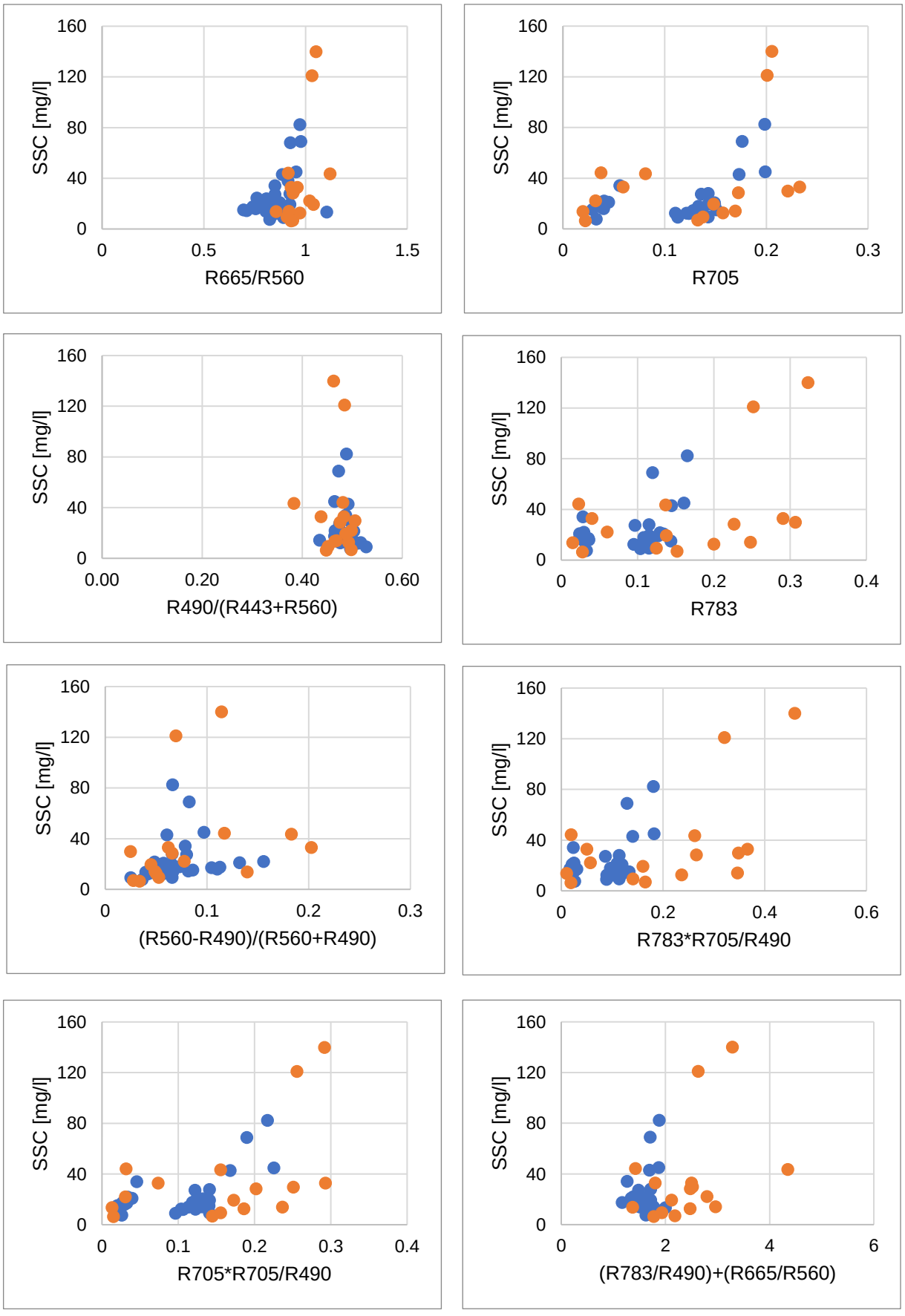

Figure 8b: Comparison of models (blue: Danube, orange: Raba) (part 2)

Table 6: Results of model comparison

Model	R^2 (Danube)	R^2 (Raba)
R705	0.69	0.20
R705*R705/R490	0.67	0.38
R665	0.65	0.36
R705-R740	0.64	0.28
R783*R705/R490	0.54	0.50
R783	0.45	0.35
R665/R560	0.15	0.28
(R560+R705)/(R560+R665)	0.10	0.02
(R783/R490) + (R665/R560)	0.08	0.15
R783/R490	0.06	0.13
(R560-R490)/(R560+R490)	0.06	0.24
R490/(R443+R560)	0.04	0.003

4. Discussion

In total we used 99 in-situ measurements for the calibration purposes. The SSC varied between 10-110 mg/l in Danube. At times of flood the values were as high as 15,000 mg/l. Those values were treated as outliers and are excluded in this study. In Raba the SSC values do not follow any predicable trend and lies between 7-16,000 mg/l. In this regard, we continued our study to consider Danube more reliable for this study. Further in this section, we will delve into additional explanations for the exclusion of Raba's values. From now on, this study will explain about the results which are the basis of why we accepted R705-R740 to be promising and useful for further study.

For Danube, satellite images from 50 different days were selected between 2nd of May 2022 and 31st of July 2023. Out of thousands of available in-situ measurements, images were selected considering the best resolution, minimal cloud cover and at the same time reliable in-situ data. For each selected day it is necessary to have parameters, such as flow discharge, SSC in-situ (daily average) and SSC in-situ (the time when image was taken), to be readily available. All the images we studied were taken at time 00:00. For every satellite image, SSC in-situ daily average was calculated. Following the methodology described in Section 2.3 and with the help of QGIS, reflectance values were extracted for each date. Spectral reflectance is defined as the ratio of radiant flux reflected from an object or area to the incident radiant flux, which is measured across specific wavelengths (Peddle, 2001). Further, using these

reflectance values Normalized difference turbidity index (NDTI) was determined and studied. The relation which was first studied under the NDTI context was (R665-R560)/(R665+R560) or (red-green)/(red+green). Here, studying a model means setting up a relation between the model itself and the SSC in-situ values (when the image was taken). Further, being inspired by previous studies, different models were calculated and studied. Among these options, the model R705-R740 demonstrated the best fit for the river Danube. The exponential trendline gives the highest value of R^2. The R^2 for this model is 0.63.

For illustration purposes, we selected a satellite image for a certain hydrological situation and created a contour map of SSC for the Danube River as shown in Figure 9. Red contours show 61 mg/l SSC whereas blue color show 72.2 mg/l SSC. All these values are for R705-R740 model. We also have onsite in-situ values as well for the day which is 9th October 2022. If comparison is made between the SSC values extract from satellite images and the onsite SSC value, then result is that the satellite images is extracting somewhat accurate values near to the in-situ values. This result indicates that for the estimation of SSC values, remote sensing can be used. The precision of the results depends on certain conditions like clouds, rate of flow and flood.

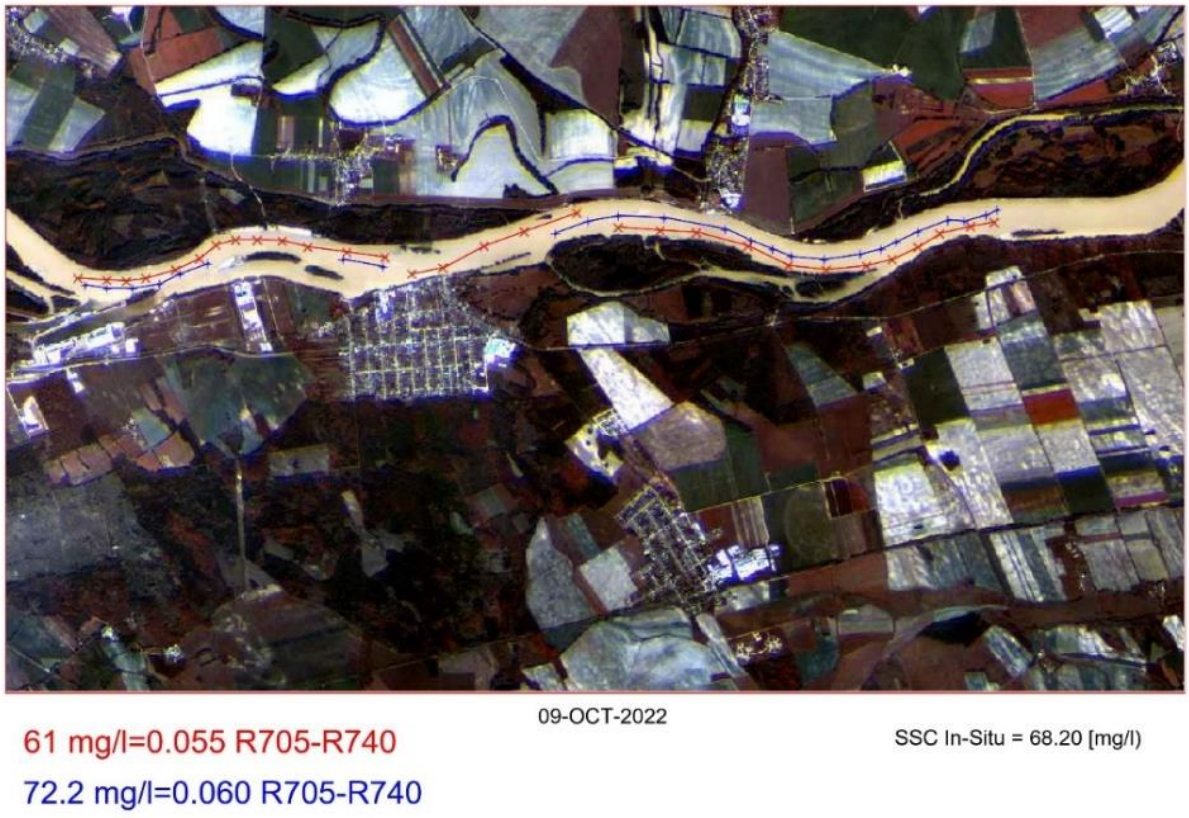

Figure 9: Contours drawn on Danube.

The main result of our study is that we worked out a procedure which produces suspended sediment concentration maps for rivers, based on the satellite imagery. For this, we apply Sentinel-2A images. Using a suitable geoinformatics environment (QGIS), we can easily download images for any day (note that the returning period of the satellites is around one week), georeference them, extract the necessary reflectance values and based on a calibration function, we can produce the SSC map. Within this study, we tested several calibration functions, from the related literature, and selected the most appropriate one for this study site.

As a future step for this study, a comprehensive assessment of SSC maps can be performed. Areal and temporal variation of SSC can be revealed, playing a crucial role in several sediment related studies. For instance, the calibrated method enables the analysis of the sediment trapping effect of reservoirs or other river elements, where sedimentation processes take place. If sedimentation occurs, the color of the river in the satellite image changes, leading to the variation of the reflectance values and eventually the SSC. Another application area of the SSC mapping can be the assessment of mixing processes at river confluences, where the different colors of the merging rivers are apparent, thus, the spatial variation of the plume from the tributary inflow can be easily outlined. Furthermore, complex suspended sediment patterns, such as the ones take place in reservoirs due to the influence of winds (see e.g., Figure 10) can be quantitatively analyzed, providing good quality input data for numerical modelling activities.

Figure 10: Spatially complex patterns of sediments in the Tisza Lake, due to wind effects

Acknowledgements

The research presented in the study was carried out within the framework of the Széchenyi Plan Plus program with the support of the RRF 2.3.1 21 2022 00008 project.

References

Chelotti, G. M. (2019). Space-Temporal analysis of suspended sediment in low concentration reservoir by Remote Sensors. 143-151.

Budapest University of Technology. (2018). Sediment Monitoring in the Danube River.

Chavez. (1988). An improved dark-object subtraction technique for atmospheric scattering correction of multispectral data.

Chelotti, G., Martinez, J., Roig, H., & Olivietti, D. (2019). Space-Temporal analysis of suspended sediment in low concentration reservoir by Remote Sensors. 143-151.

Cheng, Z., Wang, X., Paull, D., & Gao, J. (2016). Application of the Geostationary Ocean Color Imager to Mapping the Diurnal and Seasonal Variability of Surface Suspended Matter in a Macro-Tidal Estuary.

Congedo, L. (2016). *Semi-Automatic Classification Plugin User Manual.*

Curran, P., & Novo, E. (2022). The Relationship Between Suspended Sediment Concentration and Remotely Sensed Spectral Radiance. 1-25.

Gholizadeh, M., Melesse, A., & Reddi, L. (2016). A Comprehensive Review on Water Quality Parameters Estimation Using Remote Sensing.

Gualtier, C. F. (2018). A field study of the confluence between Negro and Solimões Rivers. Part 1: Hydrodynamics and sediment transport. . 1-42.

Gualtier, C., Filizola, N., Oliveira, M. d., Santos, A. M., & Ianniruberto, M. (2018). A field study of the confluence between Negro and Solimões Rivers. Part 1: Hydrodynamics and sediment transport. 1-42.

John A. Moody, B. M. (1991). Evaluation of the depth-integration method of measuring water discharge in large rivers.

Luo, W., Shen, F., He, Q., Cao, F., Zhao, H., & Li, M. (2022). Changes in suspended sediments in the Yangtze River Estuary from 1984 to 2020: Responses to basin and estuarine engineering constructions.

Muste, M., Kim, Y. (2003). Practical aspects of ADCP data use for quantification of mean river flow characteristics; Part I: moving-vessel measurements.

Mohsen, A., Kovács, F., Mezős, G., & Kiss, T. (2021). Sediment Transport Dynamism in the Confluence Area of TwoRivers Transporting Mainly Suspended Sediment Based onSentinel-2 Satellite Images. 1-30.

Peddle, D. R. (2001). Reflectance processing of remote sensing spectroradiometer data.

Qiu, Z., Xiao, C., Perrie, W., Sun, D., Wang, S., Shen, H., . . . He, Y. (2017). Using Landsat 8 data to estimate suspended particulate matter in the Yellow River estuary: Landsat 8 spm in the yellow river estuary. 276-290.

Segarra, J. (2020). Remote Sensing for Precision Agriculture: Sentinel-2 Improved Features and Applications.

Yuan, S., Tang, H., Li, K., Xu, L., Xiao, Y., Gualtieri, C., . . . Melville, B. (2021). Hydrodynamics, Sediment Transport and Morphological Features at the Confluence Between the Yangtze River and the Poyang Lake. 1-24.

Zhan, W., Wu, J., Wei, X., Tang, S., & Zhan, H. (2019). patio-temporal variation of the suspended sediment concentration in the Pearl River. 22-32.

Appendix

Date	for Danube		Date	for Raba	
	(R560-490)/(R560+490)	SSC IN-SITU (when image was taken) [mg/l]		(R560-490)/(R560+490)	SSC IN-SITU (when image was taken) [mg/l]
5/12/2022	0.05	102.42	5/12/2022	0.18	43.50
6/26/2022	0.16	21.90	6/26/2022	0.20	32.90
7/1/2022	0.08	34.10	7/1/2022	0.12	44.20
7/6/2022	0.13	20.90	8/5/2022	0.00	133.00
7/21/2022	0.10	17.10	8/10/2022	0.09	340.00
8/5/2022	0.09	15.10	7/6/2022	0.17	115.00
8/10/2022	0.11	16.00	8/30/2022	0.14	13.70
8/30/2022	0.11	17.50	7/11/2023	0.06	122.00
11/3/2022	0.04	12.20	11/3/2022	0.03	6.45
11/8/2022	0.05	12.20	11/8/2022	0.04	40.50
12/13/2022	0.03	9.10	12/13/2022	0.05	12.60
12/18/2022	0.04	7.58	1/12/2023	0.04	19.40
1/7/2023	0.07	14.20	2/21/2023	0.05	9.39
1/12/2023	0.06	12.40	3/3/2023	0.03	6.89
1/17/2023	0.08	14.40	4/12/2023	0.05	14.00
2/21/2023	0.07	27.90	5/22/2023	0.07	121.00
2/26/2023	0.07	19.40	6/1/2023	0.07	28.40
3/3/2023	0.07	9.38	6/16/2023	0.11	140.00
3/18/2023	0.07	12.30	7/11/2023	0.06	32.90
4/12/2023	0.04	13.40			
5/22/2023	0.07	82.40			
5/27/2023	0.10	45.00			
6/1/2023	0.06	42.90			
6/11/2023	0.08	69.00			
6/16/2023	0.08	27.30			
6/21/2023	0.06	19.10			
6/26/2023	0.07	17.80			
7/6/2023	0.05	13.90			
7/11/2023	0.06	15.00			
7/16/2023	0.06	20.60			
7/31/2023	0.05	21.50			

	For Danube			For Raba	
Date	R783/R490	SSC IN-SITU (when image was taken) [mg/l]	Date	R783/R490	SSC IN-SITU (when image was taken) [mg/l]
5/12/2022	0.86	102.42	5/12/2022	3.23	43.50
6/26/2022	0.61	21.90	6/26/2022	0.84	32.90
7/1/2022	0.41	34.10	7/1/2022	0.51	44.20
7/6/2022	0.47	20.90	8/5/2022	0.65	133.00
7/21/2022	0.80	17.10	8/10/2022	1.10	340.00
8/5/2022	0.70	15.10	7/6/2022	1.66	115.00
8/10/2022	0.67	16.00	8/30/2022	0.52	13.70
8/30/2022	0.43	17.50	7/11/2023	1.72	122.00
11/3/2022	0.78	12.20	11/3/2022	0.85	6.45
11/8/2022	0.79	12.20	11/8/2022	1.59	40.50
12/13/2022	0.79	9.10	12/13/2022	1.50	12.60
12/18/2022	0.80	7.58	1/12/2023	1.08	19.40
1/7/2023	0.86	14.20	2/21/2023	1.02	9.39
1/12/2023	0.81	12.40	3/3/2023	1.25	6.89
1/17/2023	0.82	14.40	4/12/2023	2.04	14.00
2/21/2023	0.79	27.90	5/22/2023	1.60	121.00
3/3/2023	0.79	9.38	6/1/2023	1.54	28.40
3/18/2023	0.92	12.30	6/16/2023	2.23	140.00
4/12/2023	0.89	13.40	7/11/2023	1.57	32.90
5/22/2023	0.91	82.40			
5/27/2023	0.92	45.00			
6/1/2023	0.81	42.90			
6/11/2023	0.73	69.00			
6/16/2023	0.64	27.30			
6/21/2023	0.79	19.10			
6/26/2023	0.72	17.80			
7/6/2023	0.70	13.90			
7/11/2023	0.88	15.00			
7/16/2023	0.80	20.60			
7/31/2023	0.74	21.50			

For Danube			For Raba		
Date	R665	SSC IN-SITU (when image was taken) [mg/l]	Date	R665	SSC IN-SITU (when image was taken) [mg/l]
5/12/2022	0.03	102.42	5/12/2022	0.07	43.50
6/26/2022	0.05	21.90	6/26/2022	0.07	32.90
7/1/2022	0.07	34.10	7/1/2022	0.05	44.20
7/6/2022	0.06	20.90	8/5/2022	0.02	133.00
7/21/2022	0.06	23.90	8/10/2022	0.03	115.00
8/5/2022	0.04	17.10	7/6/2022	0.03	13.70
8/10/2022	0.04	15.10	8/30/2022	0.05	122.00
8/30/2022	0.05	16.00	7/11/2023	0.04	22.10
11/3/2022	0.06	24.40	11/3/2022	0.14	40.50
11/8/2022	0.05	17.50	11/8/2022	0.14	12.60
12/13/2022	0.04	14.50	12/13/2022	0.14	19.40
12/18/2022	0.23	68.20	1/12/2023	0.12	9.39
1/7/2023	0.13	12.20	2/21/2023	0.12	6.89
1/12/2023	0.14	12.20	3/3/2023	0.12	14.00
1/17/2023	0.12	9.10	4/12/2023	0.19	29.80
2/21/2023	0.04	7.58	5/22/2023	0.16	28.40
2/26/2023	0.14	14.20	6/1/2023	0.19	140.00
3/3/2023	0.12	12.40	6/16/2023	0.19	32.90
3/18/2023	0.14	14.40			
4/12/2023	0.15	27.90			
5/22/2023	0.15	19.40			
5/27/2023	0.15	9.38			
6/1/2023	0.12	12.30			
6/11/2023	0.15	13.40			
6/16/2023	0.21	37.90			
6/21/2023	0.20	82.40			
6/26/2023	0.20	45.00			
7/6/2023	0.18	42.90			
7/11/2023	0.19	69.00			
7/16/2023	0.15	27.30			
7/31/2023	0.15	19.10			

Date	For Danube		Date	For Raba	
	(R560+R705)/(R560+R665)	SSC IN-SITU (when image was taken) [mg/l]		(R560+R705)/(R560+R665)	SSC IN-SITU (when image was taken) [mg/l]
5/12/2022	0.97	102.42	5/12/2022	1.10	43.50
6/26/2022	0.90	21.90	6/26/2022	0.93	32.90
7/1/2022	0.92	34.10	7/1/2022	0.87	44.20
7/6/2022	0.89	20.90	8/5/2022	0.88	133.00
7/21/2022	0.94	17.10	8/10/2022	0.95	340.00
8/5/2022	0.93	15.10	7/6/2022	0.91	115.00
8/10/2022	0.90	16.00	8/30/2022	0.81	13.70
8/30/2022	0.89	17.50	7/11/2023	0.91	122.00
11/3/2022	0.97	12.20	11/3/2022	0.84	6.45
11/8/2022	0.96	12.20	11/8/2022	1.08	40.50
12/13/2022	0.96	9.10	12/13/2022	1.05	12.60
12/18/2022	0.95	7.58	1/12/2023	1.01	19.40
1/7/2023	0.97	14.20	2/21/2023	1.06	9.39
1/12/2023	0.96	12.40	3/3/2023	1.05	6.89
1/17/2023	0.96	14.40	4/12/2023	1.18	14.00
2/21/2023	0.97	27.90	5/22/2023	1.04	121.00
2/26/2023	0.97	19.40	6/1/2023	1.05	28.40
3/3/2023	0.97	9.38	6/16/2023	1.04	140.00
3/18/2023	1.00	12.30	7/11/2023	1.09	32.90
4/12/2023	0.93	13.40			
5/22/2023	0.99	82.40			
5/27/2023	0.99	45.00			
6/1/2023	0.99	42.90			
6/11/2023	0.97	69.00			
6/16/2023	0.95	27.30			
6/21/2023	0.99	19.10			
6/26/2023	0.97	17.80			
7/6/2023	0.97	13.90			
7/11/2023	1.00	15.00			
7/16/2023	0.98	20.60			
7/31/2023	0.96	21.50			

	For Danube			For Raba	
Date	R665/R560	SSC IN-SITU (when image was taken) [mg/l]	Date	R665/R560	SSC IN-SITU (when image was taken) [mg/l]
5/12/2022	0.87	102.42	5/12/2022	1.12	43.50
6/26/2022	0.78	21.90	6/26/2022	0.96	32.90
7/1/2022	0.85	34.10	7/1/2022	0.91	44.20
7/6/2022	0.87	20.90	8/5/2022	0.94	133.00
7/21/2022	0.81	23.90	8/10/2022	0.91	340.00
8/5/2022	0.80	17.10	7/6/2022	0.93	115.00
8/10/2022	0.70	15.10	8/30/2022	0.86	13.70
8/30/2022	0.75	16.00	7/11/2023	0.96	122.00
11/3/2022	0.76	24.40	11/3/2022	0.93	6.45
11/8/2022	0.74	17.50	11/8/2022	0.93	40.50
12/13/2022	0.71	14.50	12/13/2022	0.97	12.60
12/18/2022	0.93	68.20	1/12/2023	1.04	19.40
1/7/2023	0.84	12.20	2/21/2023	0.91	9.39
1/12/2023	0.85	12.20	3/3/2023	0.94	6.89
1/17/2023	0.89	9.10	4/12/2023	0.92	14.00
2/21/2023	0.82	7.58	5/22/2023	1.03	121.00
2/26/2023	0.91	14.20	6/1/2023	0.94	28.40
3/3/2023	0.92	12.40	6/16/2023	1.05	140.00
3/18/2023	0.90	14.40	7/11/2023	0.93	32.90
4/12/2023	0.92	27.90			
5/22/2023	0.92	19.40			
5/27/2023	0.92	9.38			
6/1/2023	0.89	12.30			
6/11/2023	1.10	13.40			
6/16/2023	0.91	37.90			
6/21/2023	0.97	82.40			
6/26/2023	0.95	45.00			
7/6/2023	0.89	42.90			
7/11/2023	0.98	69.00			
7/16/2023	0.85	27.30			
7/31/2023	0.84	19.10			

	For Danube			For Raba	
Date	R705	SSC IN-SITU (when image was taken) [mg/l]	Date	R705	SSC IN-SITU (when image was taken) [mg/l]
5/12/2022	0.03	102.42	5/12/2022	0.0812	43.5
6/26/2022	0.04	21.90	6/26/2022	0.06	32.90
7/1/2022	0.06	34.10	7/1/2022	0.04	44.20
7/6/2022	0.04	20.90	8/5/2022	0.02	133.00
7/21/2022	0.04	17.10	8/10/2022	0.03	340.00
8/5/2022	0.03	15.10	7/6/2022	0.02	115.00
8/10/2022	0.04	16.00	8/30/2022	0.02	13.70
8/30/2022	0.04	17.50	7/11/2023	0.04	122.00
11/3/2022	0.12	12.20	11/3/2022	0.02	6.45
11/8/2022	0.12	12.20	11/8/2022	0.16	40.50
12/13/2022	0.11	9.10	12/13/2022	0.16	12.60
12/18/2022	0.03	7.58	1/12/2023	0.15	19.40
1/7/2023	0.13	14.20	2/21/2023	0.14	9.39
1/12/2023	0.11	12.40	3/3/2023	0.13	6.89
1/17/2023	0.13	14.40	4/12/2023	0.17	14.00
2/21/2023	0.14	27.90	5/22/2023	0.20	121.00
2/26/2023	0.14	19.40	6/1/2023	0.17	28.40
3/3/2023	0.14	9.38	6/16/2023	0.21	140.00
3/18/2023	0.12	12.30	7/11/2023	0.23	32.90
4/12/2023	0.13	13.40			
5/22/2023	0.20	82.40			
5/27/2023	0.20	45.00			
6/1/2023	0.17	42.90			
6/11/2023	0.18	69.00			
6/16/2023	0.14	27.30			
6/21/2023	0.15	19.10			
6/26/2023	0.13	17.80			
7/6/2023	0.14	13.90			
7/11/2023	0.15	15.00			
7/16/2023	0.15	20.60			
7/31/2023	0.15	21.50			

	For Danube			
	R705-R740	SSC IN-SITU (when image was taken)		R705-R740
Date		[mg/l]	Date	
5/12/2022	0.00	102.42	5/12/2022	-0.04
6/26/2022	0.02	21.90	6/26/2022	0.02
7/1/2022	0.03	34.10	7/1/2022	0.01
7/6/2022	0.02	20.90	8/5/2022	-0.02
7/21/2022	0.00	17.10	8/10/2022	0.00
8/5/2022	0.00	15.10	7/6/2022	0.00
8/10/2022	0.01	16.00	8/30/2022	0.01
8/30/2022	0.02	17.50	7/11/2023	-0.03
11/3/2022	0.01	12.20	11/3/2022	0.00
11/8/2022	0.01	12.20	11/8/2022	-0.05
12/13/2022	0.01	9.10	12/13/2022	-0.03
12/18/2022	0.00	7.58	1/12/2023	0.01
1/7/2023	0.02	14.20	2/21/2023	0.01
1/12/2023	0.02	12.40	3/3/2023	-0.02
1/17/2023	0.02	14.40	4/12/2023	-0.06
2/21/2023	0.03	27.90	5/22/2023	-0.03
2/26/2023	0.03	19.40	6/1/2023	-0.04
3/3/2023	0.03	9.38	6/16/2023	-0.07
3/18/2023	0.01	12.30	7/11/2023	-0.03
4/12/2023	0.01	13.40		
5/22/2023	0.04	82.40		
5/27/2023	0.04	45.00		
6/1/2023	0.03	42.90		
6/11/2023	0.06	69.00		
6/16/2023	0.04	27.30		
6/21/2023	0.02	19.10		
6/26/2023	0.03	17.80		
7/6/2023	0.02	13.90		
7/11/2023	0.01	15.00		
7/16/2023	0.02	20.60		
7/31/2023	0.02	21.50		

	For Danube			For Raba	
Date	(R443-R665)/(R560-R665)	SSC IN-SITU (when image was taken) [mg/l]	Date	(R443-R665)/(R560-R665)	SSC IN-SITU (when image was taken) [mg/l]
5/12/2022	0.40	102.42	5/12/2022	-0.18	43.50
6/26/2022	-0.92	21.90	6/26/2022	-0.29	32.90
7/1/2022	-0.64	34.10	7/1/2022	-0.17	44.20
7/6/2022	-2.04	20.90	8/5/2022	0.01	133.00
7/21/2022	-0.58	17.10	8/10/2022	-0.10	340.00
8/5/2022	-0.03	15.10	7/6/2022	-0.19	115.00
8/10/2022	-0.20	16.00	8/30/2022	-0.14	13.70
8/30/2022	-0.09	17.50	7/11/2023	0.03	122.00
11/3/2022	-0.23	12.20	11/3/2022	0.07	6.45
11/8/2022	-0.59	12.20	11/8/2022	-0.02	40.50
12/13/2022	-0.83	9.10	##########	-0.07	12.60
12/18/2022	0.28	7.58	1/12/2023	-0.09	19.40
1/7/2023	-0.83	14.20	2/21/2023	0.04	9.39
1/12/2023	-2.46	12.40	3/3/2023	-0.02	6.89
1/17/2023	0.53	14.40	4/12/2023	0.01	14.00
2/21/2023	-2.20	27.90	5/22/2023	-0.13	121.00
2/26/2023	-2.20	19.40	6/1/2023	-0.05	28.40
3/3/2023	-2.20	9.38	6/16/2023	-0.20	140.00
3/18/2023	-0.40	12.30	7/11/2023	-0.06	32.90
4/12/2023	1.42	13.40			
5/22/2023	-6.63	82.40			
5/27/2023	-3.99	45.00			
6/1/2023	-0.75	42.90			
6/11/2023	-7.91	69.00			
6/16/2023	-0.37	27.30			
6/21/2023	-0.37	19.10			
6/26/2023	-0.15	17.80			
7/6/2023	-0.02	13.90			
7/11/2023	-0.19	15.00			
7/16/2023	0.15	20.60			
7/31/2023	-0.18	21.50			

	For Danube			For Raba	
Date	R490/(R443+R560)	SSC IN-SITU (when image was taken) [mg/l]	Date	R490/(R443+R560)	SSC IN-SITU (when image was taken) [mg/l]
5/12/2022	0.47	102.42	5/12/2022	0.38	43.50
6/26/2022	0.47	21.90	6/26/2022	0.44	32.90
7/1/2022	0.49	34.10	7/1/2022	0.48	44.20
7/6/2022	0.48	20.90	8/5/2022	0.51	133.00
7/21/2022	0.48	17.10	8/10/2022	0.44	115.00
8/5/2022	0.50	15.10	7/6/2022	0.47	13.70
8/10/2022	0.47	16.00	8/30/2022	0.44	122.00
8/30/2022	0.46	17.50	7/11/2023	0.50	22.10
11/3/2022	0.51	12.20	11/3/2022	0.49	40.50
11/8/2022	0.51	12.20	11/8/2022	0.49	12.60
12/13/2022	0.53	9.10	12/13/2022	0.49	19.40
12/18/2022	0.50	7.58	1/12/2023	0.45	9.39
1/7/2023	0.48	14.20	2/21/2023	0.50	6.89
1/12/2023	0.52	12.40	3/3/2023	0.47	14.00
1/17/2023	0.43	14.40	4/12/2023	0.51	29.80
2/21/2023	0.50	27.90	5/22/2023	0.48	28.40
2/26/2023	0.50	19.40	6/1/2023	0.46	140.00
3/3/2023	0.50	9.38	6/16/2023	0.48	32.90
3/18/2023	0.48	12.30			
4/12/2023	0.47	13.40			
5/22/2023	0.49	82.40			
5/27/2023	0.46	45.00			
6/1/2023	0.49	42.90			
6/11/2023	0.47	69.00			
6/16/2023	0.47	27.30			
6/21/2023	0.49	19.10			
6/26/2023	0.48	17.80			
7/6/2023	0.50	13.90			
7/11/2023	0.50	15.00			
7/16/2023	0.48	20.60			
7/31/2023	0.50	21.50			

	For Danube			For Raba	
Date	R783	SSC IN-SITU (when image was taken) [mg/l]	Date	R783	SSC IN-SITU (when image was taken) [mg/l]
5/12/2022	0.02	102.42	5/12/2022	0.14	43.50
6/26/2022	0.03	21.90	6/26/2022	0.04	32.90
7/1/2022	0.03	34.10	7/1/2022	0.02	44.20
7/6/2022	0.02	20.90	8/5/2022	0.02	133.00
7/21/2022	0.04	17.10	8/10/2022	0.03	340.00
8/5/2022	0.03	15.10	7/6/2022	0.04	115.00
8/10/2022	0.04	16.00	8/30/2022	0.02	13.70
8/30/2022	0.02	17.50	7/11/2023	0.08	122.00
11/3/2022	0.11	12.20	11/3/2022	0.03	6.45
11/8/2022	0.11	12.20	11/8/2022	0.22	40.50
12/13/2022	0.10	9.10	12/13/2022	0.20	12.60
12/18/2022	0.03	7.58	1/12/2023	0.14	19.40
1/7/2023	0.12	14.20	2/21/2023	0.12	9.39
1/12/2023	0.10	12.40	3/3/2023	0.15	6.89
1/17/2023	0.11	14.40	4/12/2023	0.25	14.00
2/21/2023	0.12	27.90	5/22/2023	0.25	121.00
2/26/2023	0.12	19.40	6/1/2023	0.23	28.40
3/3/2023	0.12	9.38	6/16/2023	0.32	140.00
3/18/2023	0.11	12.30	7/11/2023	0.29	32.90
4/12/2023	0.12	13.40			
5/22/2023	0.17	82.40			
5/27/2023	0.16	45.00			
6/1/2023	0.14	42.90			
6/11/2023	0.12	69.00			
6/16/2023	0.10	27.30			
6/21/2023	0.13	19.10			
6/26/2023	0.11	17.80			
7/6/2023	0.12	13.90			
7/11/2023	0.14	15.00			
7/16/2023	0.13	20.60			
7/31/2023	0.13	21.50			

	For Danube			For Raba	
Date	R783*R705/R490	SSC IN-SITU (when image was taken) [mg/l]	Date	R783*R705/R490	SSC IN-SITU (when image was taken) [mg/l]
5/12/2022	0.02	102.42	5/12/2022	0.26	43.50
6/26/2022	0.02	21.90	6/26/2022	0.05	32.90
7/1/2022	0.02	34.10	7/1/2022	0.02	44.20
7/6/2022	0.02	20.90	8/5/2022	0.01	133.00
7/21/2022	0.03	17.10	8/10/2022	0.03	340.00
8/5/2022	0.02	15.10	7/6/2022	0.04	115.00
8/10/2022	0.03	16.00	8/30/2022	0.01	13.70
8/30/2022	0.02	17.50	7/11/2023	0.07	122.00
11/3/2022	0.10	12.20	11/3/2022	0.02	6.45
11/8/2022	0.10	12.20	11/8/2022	0.26	40.50
12/13/2022	0.09	9.10	12/13/2022	0.24	12.60
12/18/2022	0.03	7.58	1/12/2023	0.16	19.40
1/7/2023	0.12	14.20	2/21/2023	0.14	9.39
1/12/2023	0.09	12.40	3/3/2023	0.17	6.89
1/17/2023	0.10	14.40	4/12/2023	0.35	14.00
2/21/2023	0.11	27.90	5/22/2023	0.32	121.00
2/26/2023	0.11	19.40	6/1/2023	0.27	28.40
3/3/2023	0.11	9.38	6/16/2023	0.46	140.00
3/18/2023	0.11	12.30	7/11/2023	0.37	32.90
4/12/2023	0.12	13.40			
5/22/2023	0.18	82.40			
5/27/2023	0.18	45.00			
6/1/2023	0.14	42.90			
6/11/2023	0.13	69.00			
6/16/2023	0.09	27.30			
6/21/2023	0.12	19.10			
6/26/2023	0.10	17.80			
7/6/2023	0.10	13.90			
7/11/2023	0.13	15.00			
7/16/2023	0.12	20.60			
7/31/2023	0.11	21.5			

	For Danube			For Raba	
Date	R705*R705/R490	SSC IN-SITU (when image was taken) [mg/l]	Date	R705*R705/R490	SSC IN-SITU (when image was taken) [mg/l]
5/12/2022	0.02	102.42	5/12/2022	0.16	43.50
6/26/2022	0.03	21.90	6/26/2022	0.07	32.90
7/1/2022	0.05	34.10	7/1/2022	0.03	44.20
7/6/2022	0.04	20.90	8/5/2022	0.01	133.00
7/21/2022	0.03	17.10	8/10/2022	0.03	340.00
8/5/2022	0.02	15.10	7/6/2022	0.03	115.00
8/10/2022	0.03	16.00	8/30/2022	0.01	13.70
8/30/2022	0.03	17.50	7/11/2023	0.04	122.00
11/3/2022	0.10	12.20	11/3/2022	0.01	6.45
11/8/2022	0.11	12.20	11/8/2022	0.19	40.50
12/13/2022	0.10	9.10	12/13/2022	0.19	12.60
12/18/2022	0.03	7.58	1/12/2023	0.17	19.40
1/7/2023	0.13	14.20	2/21/2023	0.16	9.39
1/12/2023	0.10	12.40	3/3/2023	0.14	6.89
1/17/2023	0.13	14.40	4/12/2023	0.24	14.00
2/21/2023	0.14	27.90	5/22/2023	0.26	121.00
2/26/2023	0.14	19.40	6/1/2023	0.20	28.40
3/3/2023	0.14	9.38	6/16/2023	0.29	140.00
3/18/2023	0.12	12.30	7/11/2023	0.29	32.90
4/12/2023	0.14	13.40			
5/22/2023	0.22	82.40			
5/27/2023	0.23	45.00			
6/1/2023	0.17	42.90			
6/11/2023	0.19	69.00			
6/16/2023	0.12	27.30			
6/21/2023	0.14	19.10			
6/26/2023	0.12	17.80			
7/6/2023	0.11	13.90			
7/11/2023	0.14	15.00			
7/16/2023	0.13	20.60			
7/31/2023	0.12	21.50			

Date	for danube (R783/R490)+R(665/R560)	SSC IN-SITU (when image was taken)	Date	FOR RABA (R783/R490)+R(665/R560)	SSC IN-SITU (when image was taken)
5/12/2022	1.73	102.4	5/12/2022	4.35	43.5
6/26/2022	1.39	21.9	6/26/2022	1.80	32.9
7/1/2022	1.26	34.1	7/1/2022	1.47	44.2
7/6/2022	1.34	20.9	8/5/2022	1.59	133
7/21/2022	1.60	17.1	8/10/2022	2.00	340
8/5/2022	1.39	15.1	7/6/2022	2.58	115
8/10/2022	1.42	16	8/30/2022	1.37	13.7
8/30/2022	1.17	17.5	7/11/2023	2.68	122
11/3/2022	1.62	12.2	11/3/2022	1.78	6.45
11/8/2022	1.64	12.2	11/8/2022	2.51	40.5
12/13/2022	1.68	9.1	12/13/2022	2.48	12.6
12/18/2022	1.62	7.58	1/12/2023	2.12	19.4
1/7/2023	1.77	14.2	2/21/2023	1.93	9.39
1/12/2023	1.73	12.4	3/3/2023	2.18	6.89
1/17/2023	1.72	14.4	4/12/2023	2.96	14
2/21/2023	1.72	27.9	5/22/2023	2.63	121
2/26/2023	1.72	19.4	6/1/2023	2.48	28.4
3/3/2023	1.72	9.38	6/16/2023	3.28	140
3/18/2023	1.81	12.3	7/11/2023	2.50	32.9
4/12/2023	2.00	13.4			
5/22/2023	1.88	82.4			
5/27/2023	1.87	45			
6/1/2023	1.70	42.9			
6/11/2023	1.71	69			
6/16/2023	1.49	27.3			
6/21/2023	1.63	19.1			
6/26/2023	1.55	17.8			
7/6/2023	1.51	13.9			
7/11/2023	1.71	15			
7/16/2023	1.63	20.6			
7/31/2023	1.58	21.5			